

# Fundamental properties, localization threshold, and the Tomonaga–Luttinger behavior of electrons in nanochains

Adam Rycerz and Jozef Spałek

Marian Smoluchowski Institute of Physics,  
Jagiellonian University, Reymonta 4, 30-059 Kraków, Poland,  
e-mail: adamr@th.if.uj.edu.pl, ufspalek@if.uj.edu.pl

the date of receipt and acceptance should be inserted later

**Abstract.** We provide a fairly complete discussion of electronic properties of a nanochain within the recently proposed approach combining *Exact Diagonalization* in the Fock space with an *Ab Initio* calculations (EDABI method). In particular, the microscopic parameters of the second-quantized Hamiltonian are determined and the evolution of the system properties is traced in a systematic manner as a function of the interatomic distance (the lattice parameter,  $R$ ). Both the many-particle ground state and the dynamical correlation functions are discussed within a single scheme. The principal physical results are: (i) the evolution of the electron momentum distribution and its analysis in terms of the Tomonaga–Luttinger scaling, (ii) the appearance of mixed metallic and insulating features (*partial localization*) for the *half-filled* band case, (iii) the appearance of a universal *renormalized* dispersion relation of electron energy, and (iv) the transformation from a *highly-conducting* nanometallic state to the *charge-ordered* nanoinsulator in the *quarter-filled* case. The analysis is performed using the adjustable Gaussian  $1s$ -like basis set composing the Wannier functions, as well as includes the *long-range* Coulomb interaction.

**PACS.** 73.63.-b Electronic transport in nanoscale materials and structures – 31.15.Ar Ab initio calculations – 71.10.Hf Lattice fermion models – 71.27.+a Strongly correlated electron systems

## 1 Introduction

Recent development in computational, as well as analytical methods has lead to a successful determination of electronic properties of semiconductors and metals starting from LDA [1], LDA+U [2], and related [3] approaches. Even strongly correlated systems, such as  $V_2O_3$  (undergoing the Mott transition) and high-temperature superconductors, have been treated in that manner [4]. However, the discussion of the metal–insulator transition of the Mott–Hubbard type is not as yet possible in a systematic manner, particularly for low-dimensional systems. These difficulties are caused by the circumstance that the electron–electron interaction is comparable, if not stronger than the single-particle energy. In effect, the procedure starting from the single-particle picture (band structure) and including subsequently the interaction via a *local* potential might not be appropriate then. In this situation, one resorts to parametrized models of correlated electrons, where the single-particle and the interaction-induced aspects of the electronic states are treated on equal footing. The single-particle wave-functions are contained in the formal expressions for the model parameters. We have proposed [5] to combine the two efforts in an exact manner, at least for some model systems.

In our method of approach (EDABI), we determine *first* rigorously the ground-state energy  $E_G$  of the system of interacting particles in occupation-number representation, that is expressed as a function of microscopic parameters. *Second*, we optimize this energy with respect to the wave-functions contained in those parameters by deriving the *self-adjusted wave equation* for them. Physically, the last step amounts to allowing the single-particle wave functions relax in the correlated state. In practice, we propose the particular class of those functions, which are obtained by minimizing the ground-state energy  $E_G$ .

The EDABI method has been overviewed in number of papers [6, 7, 8], so we concentrate here on its application to one-dimensional (1D) nanochains of  $N \leq 16$  atoms, close to the metal–insulator crossover transition. The paper complements our recent study of such systems [6, 7] with the systematic analysis of both *half-* and *quarter-filled* band cases, as well as with the analysis of its transport properties. Throughout the paper we are using the adjustable Wannier functions composed of Gaussian basis set (STO–3G), that are determined explicitly from the minimization of the system ground-state energy  $E_G$  as a function of the interatomic distance  $R$ .

The question of delocalization of atomic states has also a practical relevance. Namely, in dealing with electronic properties of quantum dots one usually assumes

the existence of the effective-mass states. The question for which systems this assumption is well founded, can be answered only by determining the critical interatomic distance, above which the states are localized. In this context, we address this question here for model systems composed of  $s$ -like states.

The structure of the paper is as follows. In the next Section we present briefly the basic idea of the EDABI method. Then, in Section 3, we provide the numerical ground-state analysis of nanochains with the long-range Coulomb interaction. Namely, we discuss the electron momentum statistical distribution function for the half-filled case and analyse it in terms of Tomonaga–Luttinger scaling (including the logarithmic correction), illustrate the charge-density wave ordering for the quarter filling, as well as analyze the  $N$ -particle wave function localization according the method developed by Resta [9]. In Section 4, we calculate the system charge and spin gaps, as well as perform the finite-size scaling with  $1/N \rightarrow 0$  on these quantities. We also analyze the spectral density and extract from it the *renormalized* dispersion relation for the interacting electrons in a nanochain. To the best of our knowledge, such an exact renormalized one-electron band structure has not been determined before. Finally, the application of the present scheme to the higher ( $ns$ -like) valence orbital systems would make possible a direct comparison with the experimental results quantum nanowires made of noble and alkaline elements. Also, the correspondence between the localization criteria inferred from the ground-state properties on one side, as well as from the dynamical correlation functions, is established there.

## 2 The combined exact diagonalization *ab initio* (EDABI) method

The basic idea of EDABI method [5,8] is illustrated on the block-diagram exhibited in Fig. 1. We start from choosing the initial Wannier basis set  $\{w_i(\mathbf{r})\}$ , composed of atomic-like wave functions (here a trial Gaussian basis set) with their radii  $a_i$ . Next, we write down the system

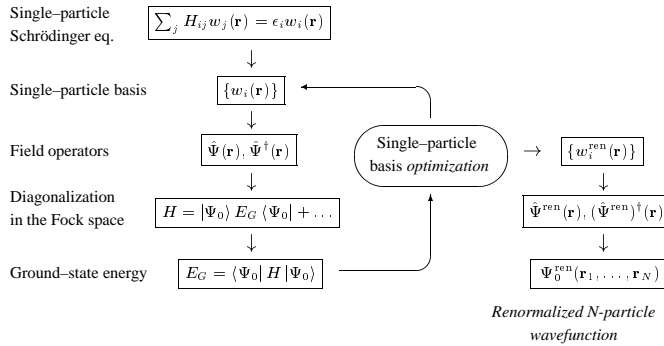


**Fig. 1.** Flowchart diagram of EDABI method. The part on the far right provides *renormalized* Wannier functions, field operators, and  $N$ -particle wave function. The top line is absent if we select the trial Wannier functions as composed of adjustable Gaussian orbitals (e.g. the STO-3G basis).

Hamiltonian in the second-quantization form and determine the ground-state energy  $E_G$  and the corresponding state in the Fock space  $|\Psi_0\rangle$  by e.g. employing the Lanczos procedure. Next, the Wannier basis set  $\{w_i(\mathbf{r})\}$  is optimized with respect to the atomic radii  $a_i$ , contained in the atomic wave functions composing  $w_i(\mathbf{r})$ , until the minimal ground-state energy  $E_G$  is reached [5] for given lattice parameter  $R$ . On the right, the renormalized quantities (for the optimized basis) are listed.

## 3 The correlated electrons in a nanochain

We consider the system of  $N_e$  electrons on  $N$  lattice sites arranged periodically, each site containing a single valence orbital and an infinite-mass ion (i.e. we start from hydrogenic-like atoms). The Hamiltonian including *all* the Coulomb-interaction terms and neglecting other (e.g. exchange terms), can be written down (up to the constant) in the form

$$H = \epsilon_a^{\text{eff}} \sum_i n_i + t \sum_{i\sigma} (a_{i\sigma}^\dagger a_{i+1\sigma} + \text{HC}) + U \sum_i n_{i\uparrow} n_{i\downarrow} + \sum_{i < j} K_{ij} \delta n_i \delta n_j, \quad (1)$$

where  $\delta n_i \equiv n_i - 1$ ,  $\epsilon_a^{\text{eff}} = \epsilon_a + N^{-1} \sum_{i < j} (2/R_{ij} + K_{ij})$  (in Ry) is the effective atomic level,  $R_{ij}$  is the distance between the  $i$ -th and  $j$ -th atoms,  $t$  is the nearest-neighbor hopping,  $U$  and  $K_{ij}$  are the intra- and inter-site Coulomb repulsions, respectively. Thus, all the *mean-field* Coulomb terms are collected in  $\epsilon_a^{\text{eff}}$ , whereas the last term in the above Hamiltonian represent the *correlation part* of the long-range interactions.

Hamiltonian (1) is diagonalized in the Fock space with the help of Lanczos technique. As the microscopic parameters  $\epsilon_a^{\text{eff}}$ ,  $t$ ,  $U$ , and  $K_{ij}$  are calculated numerically in the Gaussian basis, the orbital size of the  $1s$ -like state expressed in this basis is subsequently adjusted to obtain the minimal ground state energy  $E_G$  as a function of the interatomic distance  $R$ . Earlier, we have shown [5] that such a combined exact diagonalization – *ab initio* study of the one dimensional system provides the localization threshold, the electron–lattice couplings, and the dimerization magnitude. Moreover, the utilization of the Gaussian-type orbitals leads to variational procedure that converges rapidly with the lattice size  $N$  [7,10], so one can extrapolate the optimal orbital parameters for larger  $N$  using those obtained for small systems (i.e. for  $N = 6 \div 10$ ) and speed up the computation remarkably.

### 3.1 Statistical distribution and the Tomonaga–Luttinger scaling: The half-filled case

We discuss now the electron momentum distribution of 1D chain of  $N = 6 \div 16$  atoms to address the question whether the system composes either the *Luttinger-liquid* or forms the insulating (Mott–Hubbard) state. We first summarize,

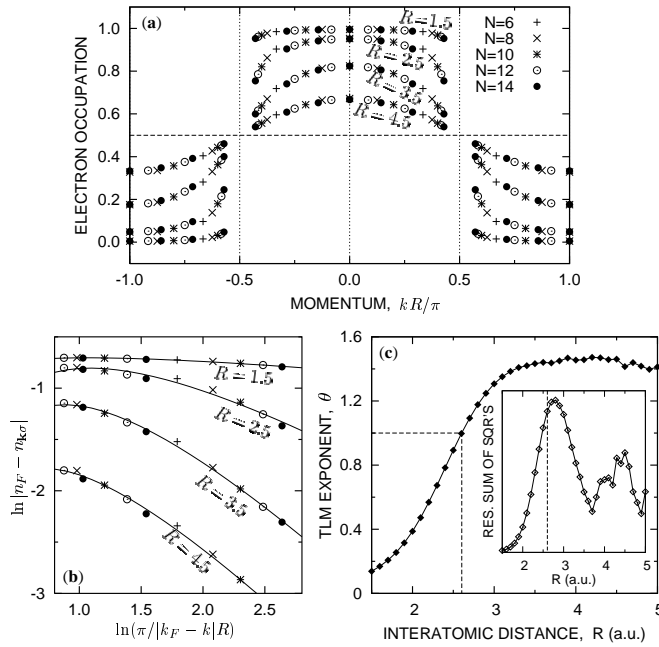


**Fig. 2.** Luttinger–liquid scaling for a *half-filled* 1D chain of  $N = 6 \div 14$  atoms with *long-range* Coulomb interactions: (a) momentum distribution for electrons in the linear and (b) log–log scale; (c) Tomonaga–Luttinger model exponent  $\theta$  vs. lattice parameter  $R$  (specified in  $a_0$ ) and (inset) the corresponding residual sum of squares. Solid lines in Figs. (a) and (b) represent the fitting of Eq. (3).

following Voit [11], the salient properties of 1D conductors, which include the two principal characteristics:

(i) A continuous momentum distribution function, showing the singularity near the Fermi level  $k \rightarrow k_F$  in the form (Solyom, Ref. [11])

$$n_{k\sigma} = n_F + A |k_F - k|^\theta \operatorname{sgn}(k_F - k), \quad (2)$$

where  $\theta$  is a non–universal (*interaction-dependent*) exponent; in consequence, it leads to the absence of fermionic quasi–particles (the quasi–particle residue in vanishes as  $z_k \sim |k_F - k|^\theta$  when  $k \rightarrow k_F$ ). In other words, the *Fermi ridge* is absent in this case.

(ii) Similar power–law behavior of all the other physical properties, particularly of the single–particle density of states  $\mathcal{N}(\omega) \sim |\omega - \mu|^\theta$  (*pseudogap*), that implies a finite Drude weight  $D > 0$  for  $\theta < 1$ .

In the case of lattice models, such as the (*extended*) Hubbard model, the Luttinger liquid behavior is predicted by the renormalization group (RG) mapping onto Tomonaga–Luttinger model [11]. Through such mapping, one can also expect, with the increasing  $N$ , the gradual convergence of the discrete momentum distribution  $n_{k\sigma}$  into the continuous power–law form (2). This hypothesis was first checked numerically for the Hubbard model by Sorella *et al.* [12].

Here we present the approach to a finite 1D chain with long–range Coulomb interaction, as described by the

**Table 1.** The parameters of the expansion (3) for the *half-filled* chain with *long-range* Coulomb interactions. The corresponding standard deviations  $\sigma$  are also specified.

$R/a_0$	$\theta$	$\sigma(\theta)$	$b$	$\sigma(b)$	$c$	$\sigma(c)$
1.5	0.138	0.015	0.147	0.024	-0.567	0.015
2.0	0.387	0.055	0.425	0.089	-0.346	0.053
2.5	0.893	0.122	0.971	0.196	0.084	0.118
3.0	1.307	0.128	1.315	0.207	0.357	0.125
4.0	1.455	0.186	1.113	0.299	-0.032	0.180
5.0	1.413	0.133	0.943	0.214	-0.823	0.129

Hamiltonian (1), with a simultaneous evaluation of the model parameters by optimizing the single–particle wave functions contained in those parameters [5]. The discrete electron–momentum distribution for the half–filling ( $N_e = N$ ) is depicted in Fig. 2a, whereas in Fig. 2b we replot it in the *log–log* scale together with the fitted theoretical curves, as explained below. In order to obtain those results we use the boundary conditions (BC) that minimize the ground–state energy for a given  $N$  (namely, the *periodic* BC for  $N = 4n + 2$  and the *antiperiodic* BC for  $N = 4n$ , at the half–filling).

To extract the exponent  $\theta$  accurately from the data for finite  $N$ , it was necessary to include also the higher scaling corrections to (2). They can be obtained from the Tomonaga mapping in the form of an expansion in the powers of  $\ln(\pi/|k_F - k|a)$ , namely,

$$\ln |n_F - n_{k\sigma}| = -\theta \ln z + b \ln \ln z + c + \mathcal{O}(1/\ln z), \quad (3)$$

where  $z \equiv \pi/|k_F - k|$ . This singular form of the expansion is required by the especially slow approach to the RG fixed point (Solyom, Ref. [11]). Obviously, by neglecting the logarithmic corrections one reaches the asymptotic form (2) for  $k \approx k_F$ . The solid lines in Fig. 2b represent the formula (3); the fitted values of the parameters  $\theta$ ,  $b$ , and  $c$  are also listed in Table 1. The quality of the fit is decessively worse for the points far away from the Fermi momentum, and depends on  $N$ , as the Fermi wave vector is  $N$ –dependent, i.e.  $k_F^N = k_F^\infty (1 - 2/N)$ , where  $k_F^\infty = \pi/(2R)$  represents the Fermi wave vector for  $N \rightarrow \infty$ . The exponent  $\theta$  is also plotted in Fig. 2c as a function of the lattice parameter  $R$  showing that it crosses the critical value  $\theta = 1$  (corresponding to the metal–insulator boundary in 1D) for  $R_c = 2.60a_0$  ( $a_0 = 0.529$  Å is the Bohr radius). We also supply the *residual sum of squares* (*cf.* inset in Fig. 2c) to show, that the fit quality becomes worst for  $R \approx R_c$ , where the system approaches the localization threshold.

The results for the half-filled system with the *on-site* Hubbard repulsion only, but with the atomic energy part included explicitly as a function of  $R$  [13], are qualitatively very similar to those displayed in Fig. 2. The critical value of the lattice parameter in that case is  $R_c = 2.16a_0$ , and also does not differ drastically from the previous one (*cf.* Table 2 for the corresponding values of all the fitted parameters in the Hubbard–model case). This is because such nanoscopic systems always have a finite conductivity in the large–density limit, since the external electron tunnels through a finite potential barrier. Therefore, such

**Table 2.** The fitted parameters of the singular expansion (3) for a half-filled 1D Hubbard chain.

$R/a_0$	$\theta$	$\sigma(\theta)$	$b$	$\sigma(b)$	$c$	$\sigma(c)$
1.5	0.229	0.030	0.237	0.048	-0.537	0.029
2.0	0.803	0.100	0.855	0.162	-0.078	0.097
2.5	1.283	0.109	1.259	0.176	0.217	0.106
3.0	1.420	0.075	1.230	0.121	0.116	0.073
4.0	1.436	0.069	1.033	0.111	-0.456	0.067
5.0	1.371	0.037	0.873	0.060	-1.218	0.036

half-filled systems, both with and without inclusion of the long-range interactions can be regarded as close to the metal–insulator transition, in no apparent contradiction with the infinite-chain RG result by Fabrizio [14], and with the Hubbard–model solution by Lieb and Wu [15]. This discussion is complete only after calculating the charge and spin gaps, as well as the electric conductivity, which are dealt with in the next two Sections.

The present analysis supplements the earlier discussion [5, 7, 10], in which we have interpreted the distribution  $n_{\mathbf{k}\sigma}$  in Fig. 2a in terms of the modified Fermi distribution for an almost localized Fermi liquid. The points are arranged in an almost flat manner for the interatomic distance  $R = 1.5a_0$  suggesting some kind of quasi-discontinuity of  $n_{\mathbf{k}\sigma}$  near  $k_F$ . However, an ambiguity arises because of the circumstance that for the nanosystems the points very close to the Fermi momentum for  $N \rightarrow \infty$  system, i.e. the point  $k_F^\infty = \pi/(2R)$ , are simply missing. Nonetheless, it is absolutely amazing that the momentum distribution can be rationalized in such simple terms (as either the Fermi or the Tomonaga–Luttinger liquids), which represent concepts borrowed from the  $N \rightarrow \infty$  limit. One should also say that the critical value of  $R_c = 2.60a_0$  for the localization of the single-particle states obtained here is about 30% lower than the corresponding value  $R_c = 3.93a_0$  obtained when we treat the distribution  $n_{\mathbf{k}\sigma}$  as the modified Fermi distribution, but the discrepancy of that order should not surprise anybody, since the localization criteria should be treated as semi-quantitative at best. One can hope to clarify the situation by extending the present analysis to larger  $N$ . Nevertheless, if we regard nanoscopic systems of  $N \sim 10$  atoms as real systems we have to deal with, then the ambiguity of the statistical distribution is to stay with us. Also, the *partial* localization of electrons in a nanosystems will become apparent when we discuss the multiparticle wave-function localization at the end of this Section and the conductivity in the next Section.

We allow ourselves for one specific suggestion (if not speculation) at this point. Namely, the results shown in Fig. 2 (and the discussion in the remaining part of the paper) point to the possibility that the system with small  $R \lesssim 2a_0$  can be analyzed as a Landau–Fermi liquid (albeit with discrete momentum states [16]), whereas the system with  $2a_0 \lesssim R \lesssim 2.5a_0$  is closer to the Tomonaga–Luttinger–Solyom limit. For  $R \gtrsim 2.5a_0$  the electrons can be regarded as effectively localized. Such a division into *three physically distinct* regimes requires a further discussion, carried out, to some extent, below.

Finally, it should be noted that a well-defined *spin-density-wave state* develops with the increasing  $R$  for the half-filled case, as discussed elsewhere [7, 13]. The system ground-state energy as a function of  $R$  is also provided there.

### 3.2 Onset of the charge–density wave state for the quarter filling

The electron quasi-momentum distribution for the *quarter-filled* (QF) case ( $N_e = N/2$ ) is shown in Fig. 3. The available number of datapoints is too small to fit the singular formula (3) to a reasonable accuracy. In effect, the lines on the plot are a guide to the eye only. However, the smooth behavior of the Luttinger–liquid type is evident for  $R \lesssim 4a_0$ , and changes dramatically for the larger values of  $R$ . This change reflects the onset of the *charge-density-wave ordering*, as illustrated in Fig. 4. In QF chain of  $N = 16$  atoms (cf. Fig. 4a) the charge is almost uniformly distributed for  $R \lesssim 3a_0$ , but the charge density wave (CDW) sets in very rapidly in the range  $R/a_0 = 4 \div 5$ . The CDW order parameter, defined as  $\theta_{\text{CDW}} \equiv$

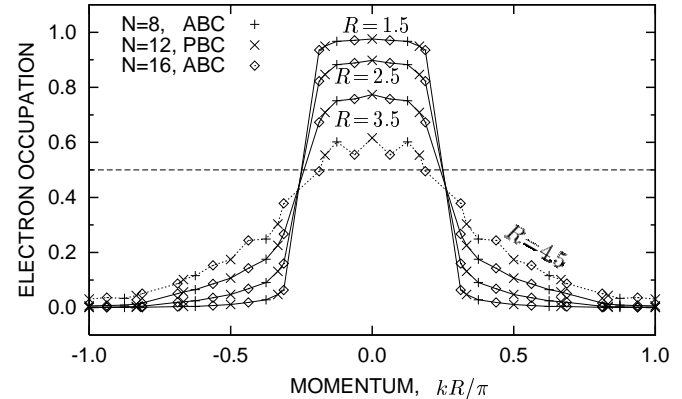


**Fig. 3.** Momentum distribution  $n_{\mathbf{k}\sigma}$  for electrons on a chain of  $N = 8 \div 16$  atoms in the *quarter-filled* case ( $N_e = N/2$ ). Lines are drawn as a guide to the eye only. ABC and PBC denotes the *antiperiodic* and *periodic* boundary conditions.

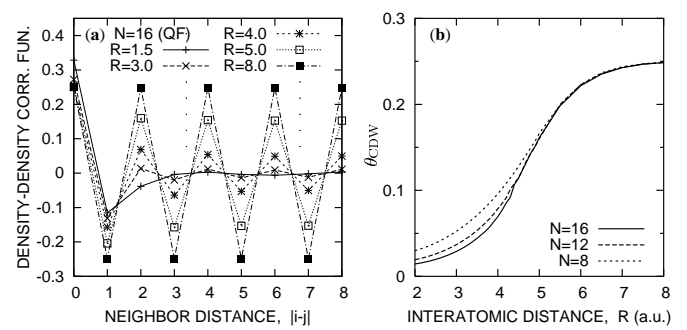


**Fig. 4.** Charge–density distribution for the *quarter-filled* ( $N_e = N/2$ ) nanochain: (a) density fluctuation correlation function  $\langle \Delta n_i \Delta n_j \rangle$  vs. distance  $|i - j|$ , (b) charge–density wave order parameter for the alternating density fluctuation (see main text for the definition) vs. interatomic distance  $R$ .

$N^{-1} \sum_m (-1)^m \langle \Delta n_i \Delta n_{i+m} \rangle$ , (where  $\Delta n \equiv n - \langle n \rangle$ ) approaches its maximal value  $\theta_{\text{CDW}} = 1/4$  for  $R \gtrsim 8a_0$  (cf. Fig. 4b). Also, the crossover range of  $R$ , where  $\theta_{\text{CDW}}$  evolves from  $\theta_{\text{CDW}} \approx 0$  to the perfect-order value  $\theta_{\text{CDW}} = 1/4$ , shrinks systematically with the increasing  $N$ , suggesting a quantum critical behavior in the large  $N$  limit. One can argue, that the charge-ordered state for larger  $R$ , corresponding to 1D *Wigner-crystal* state on a lattice, is unstable in the  $N \rightarrow \infty$  limit, in correspondence with the Mermin–Wagner theorem. Namely, we expect the amplitude of the quantum charge fluctuations to diverge at zero temperature as  $\log N$  for the system with a long-range ( $\sim 1/r$ ) Coulomb coupling. However, the divergence is absent for  $R \gtrsim 5a_0$  in the all exact-diagonalization data for  $N = 8 \div 16$  (cf. Fig. 4b), indicating that the zero-point charge fluctuations are suppressed by the onset of the CDW state. In other words, the larger lattice parameter  $R$  is, the larger system can be regarded as charge ordered in the quarter-filled case. This notion agrees with the expected atomic-limit charge-order in the QF case. The correspondence between the appearance of such charge-order and the system conductivity is discussed in the *next* Section, but first, we supplement our analysis of the system ground-state properties with the many-body wavefunction localization in the framework proposed by Resta [9].

### 3.3 Ground-state wavefunction localization

The approach [9] to the electron localization in the correlated state is based on the idea that although the insulating or the metallic states of matter are usually characterized by their excitation spectrum, the qualitative difference in *dc* conductivity must also reflect a qualitative difference in the organization of the electrons in their ground state. Such a concept was first emphasized by Kohn in a milestone paper [17], but a complete treatment, related to the Berry-phase theory of polarization, was proposed over 30 years later by Resta and Sorella (cf. Ref. [18]). In their approach the complex number

$$z_{N_e} = \langle \Psi_0 | e^{i(2\pi/L)\hat{X}} | \Psi_0 \rangle \quad (4)$$

(where  $\hat{X}$  is a many-body position operator defined in 1D as  $\hat{X} \equiv \sum_j x_j$  and  $L = NR$  is the system length) is used to discriminate between a localized  $N_e$ -particle ground state (where  $|z_{N_e}| \rightarrow 1$  for large systems) and a delocalized one, where  $z_{N_e}$  vanishes. Namely, the qualitative measure of the electron localization is defined as

$$\langle x^2 \rangle_c = -\frac{1}{N_e} \left( \frac{L}{2\pi} \right)^2 \log |z_{N_e}|^2 = -\frac{NR^2}{4\pi^2 \bar{n}} \log |z_{N_e}|^2 \quad (5)$$

(where  $\bar{n} = N_e/N$  is the average density), whereas the phase of the phase of the complex number  $z_{N_e}$  is related to the macroscopic system polarization. One should note at this point, that the kind of localization described by Eq. (5) is clearly *not* a feature characterizing the individual single-particle orbitals; instead, it is a global property of a multiparticle ground-state wavefunction *as a whole*.

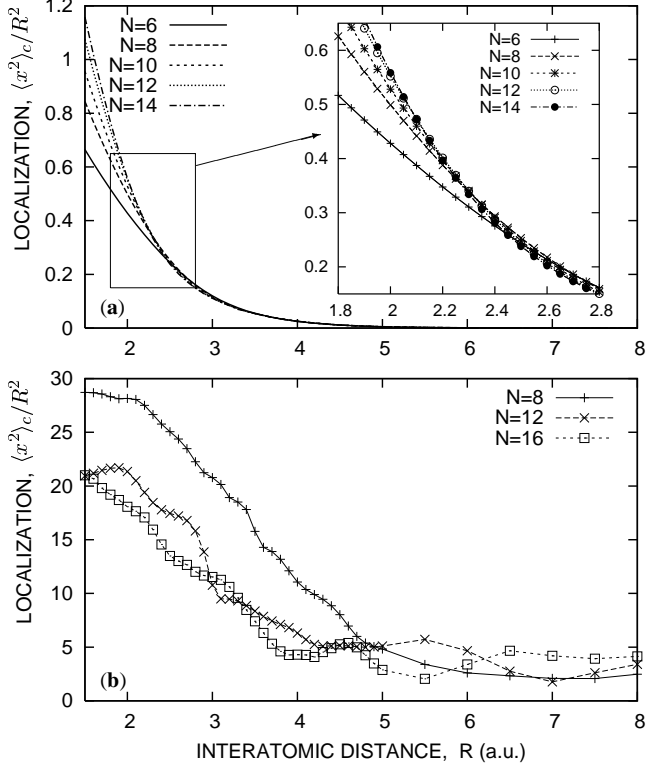


**Fig. 5.** Localization of the ground-state multiparticle wavefunction for the *half-filled* (a) and the *quarter-filled* (b) nanochains. The values of the localization parameter (see main text for the definition) are specified in the units of  $R$ .

That is because the operator  $e^{i(2\pi/L)\hat{X}}$  in Eq. (4) *cannot* be expressed as a single-particle operator (like  $\hat{X}$ ) and is rather a *genuine* many-body operator.

The numerical evaluation of the complex number  $z_{N_e}$  and the resulting  $\langle x^2 \rangle_c$  within the Lanczos algorithm is straightforward, since the operator  $e^{i(2\pi/L)\hat{X}}$  in Eq. (4) is diagonal in the position representation. The results for 1D system with long-range Coulomb interaction are shown in Fig. 5 for both the half- and the quarter-filled cases (cf. Fig. 5a and 5b, respectively). To avoid confusion by changing the system length  $L$ , we plot the localization data in the units of lattice parameter  $R$ , namely  $\langle x^2 \rangle_c / R^2$ , instead of  $\langle x^2 \rangle_c$ . The values of the localization parameter, depicted in Fig. 5a, decay gradually with growing  $R$  for all available numbers of atoms  $N$ . However, the dramatic change of the decay character takes place around the value of the lattice parameter  $R \approx 2.5a_0$  (cf. *inset* in Fig. 5a), where the curves for different  $N$  join together and forms a single one for  $R \gtrsim 2.5a_0$ . In contrast, for lower values of  $R$ , the curves are well separated, showing the divergence of the localization parameter with  $N$  for  $R \lesssim 2a_0$ . The results for the Hubbard model (not shown) again does not differ qualitatively from those presented in Fig. 5a; the coalescence point is located than near the value  $R \approx 2.2a_0$ . The positions of the joining points for both the models (with and without inclusion of the long-range Coulomb interactions) are very close to the corresponding critical

values  $R_c$  obtained from the Tomonaga–Luttinger scaling at the beginning of this Section.

The numerical results for the quarter-filled case, shown in Fig. 5b, are of lesser accuracy than those for the half-filling. This is because the complex expectation value  $z_{N_e}$ , defined by Eq. (4), is itself a sum of many complex numbers with different phases, when calculated in the position representation. If the resulting  $z_{N_e}$  is close to zero, which is the case for QF for all examined values of  $R$ ; it is, in turn, strongly affected by the computer roundoff errors, which are also amplified by taking the logarithm of  $|z_{N_e}|^2$ , when calculating  $\langle x^2 \rangle_c$  from Eq. (5). Nevertheless, the evolution of the wavefunction localization parameter versus  $R$  is qualitatively similar to that for the half-filled case: the curves for different system sizes  $N$ , depicted in Fig. 5b, get very close to each other for  $R \gtrsim 4.5a_0$ , where the charge-density wave state is formed, as discussed in the preceding subsection.

The apparent correspondence between the wavefunction localization properties and the nature of electron momentum distribution, both discussed in this Section, suggests that a significant reorganization of the ground state takes place when the nanochain is close to the localization threshold. These observations are supplemented with an analysis of the system energy gap, the spectral function, and transport properties in the *next* Section.

## 4 Spectral and transport properties

### 4.1 The charge and the spin gaps

For a further verification, whether the system is quasi-metallic or insulating in the Luttinger–liquid like regime, we perform first an extrapolation with  $1/N \rightarrow 0$  of the charge-gap defined (for the *half-filling*) as

$$\Delta E_C(N) = E_G^{N+1} + E_G^{N-1} - 2E_G^N, \quad (6)$$

where  $E_G^{N_e}$  is the ground-state energy of the system containing  $N_e$  electrons. The corresponding numerical results are shown in Fig. 6, where we use again the proper boundary conditions (*periodic* or *antiperiodic*) that minimize the ground-state energy. The extrapolation with  $1/N \rightarrow 0$  performed using the 2-nd and the 3-rd order polynomials in  $(1/N)$  provides a nonzero value of  $\Delta E_C$  for wide range of the lattice parameter  $R$ . Only for the lowest examined value of  $R = 1.5a_0$ , the gap  $\Delta E_C$  reaches zero within the extrapolation error; for  $R > 1.5a_0$  it is clearly nonvanishing. The gap is also significantly smaller than the corresponding Hartree–Fock value in the regime  $R \lesssim 4.5a_0$ , suggesting that some kind of reorganization is present in the dielectric properties, e.g. a crossover from the Slater– to the Mott–type insulator, as discussed for the parametrized models [18]. This hypothesis is verified by estimating the spin gap *below*.

The situation changes completely when we consider the *quarter-filled* band case,  $N_e = N/2$  (*cf.* Fig. 7). The parabolic extrapolation with  $1/N \rightarrow 0$  provides now the value of the charge-gap  $\Delta E_C \approx 0$  (within the errorbars)

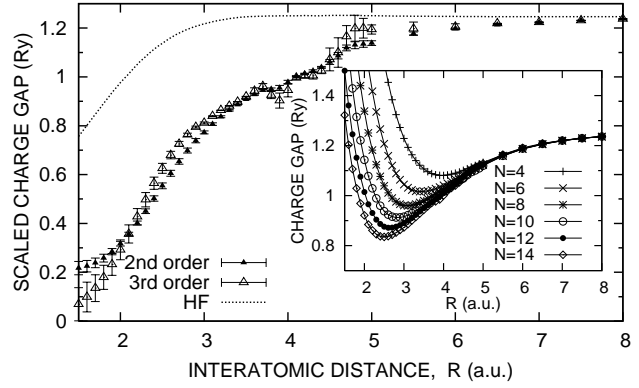


**Fig. 6.** Charge–energy gap obtained through the finite–size scaling for the chains of  $N = 4 \div 14$  atoms. The corresponding Hartree–Fock (HF) value of the magnetic gap for an infinite system is also drawn for comparison (dotted line). The *inset* exhibits the original data for different values of  $N$ , used for the scaling.

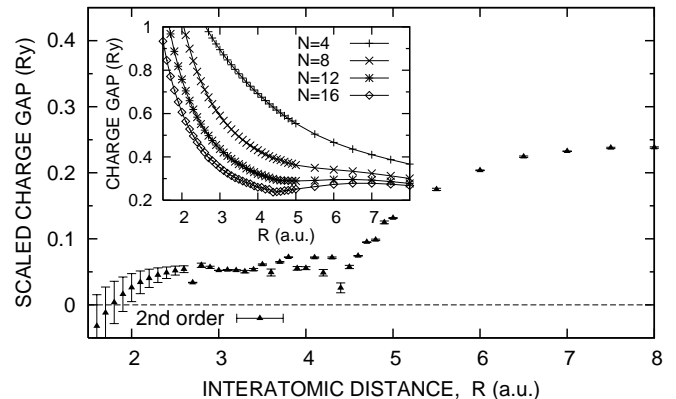


**Fig. 7.** Charge–energy gap obtained through the finite–size scaling for the chains of  $N = 4 \div 16$  atoms in the *quarter-filled* case. The 2-nd order polynomial has been fitted to perform the extrapolation with  $1/N \rightarrow \infty$ . *Inset* provides the original data used for the scaling.

for the lattice parameter  $R \lesssim 2a_0$ . In the range of  $R/a_0 = 2.5 \div 4.5$  the gap develops (it is significantly greater than the corresponding errorbars), but a random dispersion of the datapoints suggests an inaccuracy of the performed extrapolation due to the nonanalytic behavior of  $\Delta E_C$  when the system approaches the localization threshold. For  $R \gtrsim 4.5a_0$  the gap grows smoothly to a limiting value corresponding to that for the insulating charge–density wave state, identified earlier. The more precise position of the localization point is determined later in this Section, where we calculate the system Drude weight.

For a sake of completeness we now provide, in Fig. 8, the values of the system *spin gap*, which is defined as

$$\Delta E_S \equiv E_G(S_z = 1) - E_G(S_z = 0), \quad (7)$$

where  $E_G(S_z)$  denotes the lowest eigenenergy in the subspace with a given total  $z$ –component of spin  $S_z$ . Through the finite–size scaling with  $1/N \rightarrow 0$ , we obtain the spin gap  $\Delta E_S \approx 0$  for both the half– and the

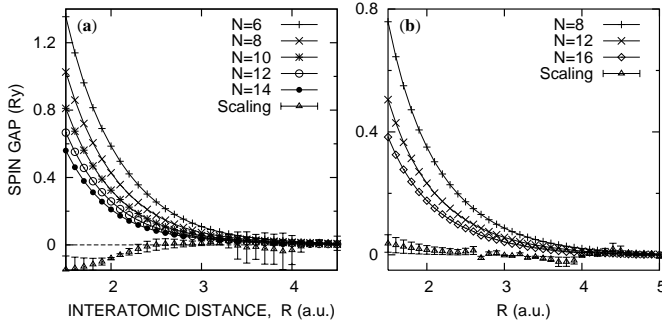


**Fig. 8.** Spin gap for the *half-filled* (a) and the *quarter-filled* (b) nanochains. The results obtained through the finite-size scaling are also shown with the corresponding errorbars.

quarter-filled cases (cf. Figs. 8a and 8b, respectively) and in the whole examined range of the interatomic distance  $R$ . These results show clearly that the insulating phase of the system is of the Mott type in the large- $N$  limit. No indications of the Slater-type phase, for which  $\Delta E_C = \Delta_S > 0$ , was found. However, for a nanosystem containing  $N \sim 10$  atoms, one can note that the so-called *correlated insulator* ( $\Delta E_C > \Delta_S > 0$ ), existing for the small values of  $R$  (cf. insets to Figs. 6 and 7, and Fig. 8) transforms gradually into the Mott insulator with the increasing  $R$ . This evolution should be contrasted with the evolution of bulk three-dimensional systems where the Slater antiferromagnet evolves into the Mott insulator.

#### 4.2 Spectrum of single-particle excitations: renormalized bands vs. Hubbard subbands

The evolution of the single-particle spectral density function  $A_{\mathbf{k}}(\omega)$  with the increasing  $R$  is shown in Fig. 9a for the *half-filled* ( $N_e = N$ ) nanochain described by the Hamiltonian (1). The spectral function is defined in the standard manner, namely

$$A_{\mathbf{k}}(\omega) = \sum_n \left| \langle \Psi_n^{N \pm 1} | c_{\mathbf{k}\sigma}^{\pm} | \Psi_0^N \rangle \right|^2 \delta [\omega - (E_n^{N \pm 1} - E_0^N)], \quad (8)$$

where the upper (lower) sign correspond to  $\omega > \mu$  ( $\omega < \mu$ ), respectively,  $|\Psi_n^N\rangle$  is the  $n$ -th eigenstate of the system containing  $N$  particles,  $E_n^N$  is the corresponding eigenenergy, and the matrix element  $\langle \Psi_n^{N \pm 1} | c_{\mathbf{k}\sigma}^{\pm} | \Psi_0^N \rangle$ , with  $c_{\mathbf{k}\sigma}^+ \equiv a_{\mathbf{k}\sigma}^{\dagger}$  and  $c_{\mathbf{k}\sigma}^- \equiv a_{\mathbf{k}\sigma}$ , is calculated within the Lanczos technique set up by Dagotto [20]. For plotting the purposes, we have used analytical representation of Dirac delta function  $\delta(x) \rightarrow (1/\pi)\epsilon/(x^2 + \epsilon^2)$  with  $\epsilon = 0.01$  Ry. In the nanometallic range ( $R \lesssim 2.5a_0$ ), the quasiparticle peaks are well defined, but incoherent tails are always present and grow in strength with the increasing  $R$ . In effect, in the intermediate regime of  $R \sim 3a_0$  the lower and the upper Hubbard bands are formed, which, in turn, continuously evolve into discrete atomic levels located at the positions  $\omega = \epsilon_a$  and  $\omega = \epsilon_a + U$ , when  $R \rightarrow \infty$ . Those limiting peak positions correspond to the ground ( $H^0$ ) and

excited ( $H^-$ ) atomic levels. Probably, the most interesting feature of this spectrum is its incoherent nature for  $R \sim 3a_0$ , where the band and the interaction energies are comparable and where the Luttinger liquid exponent crosses the critical value  $\theta = 1$  (cf. Section 3.1), corresponding to the localization threshold.

A direct picture of the spectrum evolution is provided by the *renormalized* dispersion relation, obtained from the spectral function by extracting the major quasiparticle peak position for each momentum  $k$ , and plotted in Figs. 9b–d. We again easily identify: (i) the *nanometallic range* (cf. Fig. 9b for  $R = 1.5a_0$ ), for which the charge gap is of the same order as the energy discretization due to the geometrical quantization of the quasiparticle momenta, (ii) the *intermediate regime* (cf. Fig. 9c,  $R = 3a_0$ ) where the gap become significantly wider, and (iii) the *atomic limit* (cf. Fig. 9d,  $R = 8a_0$ ), in which two dispersionless manifolds located at the energies  $\omega = \epsilon_a$  and  $\omega = \epsilon_a + U$  appear. One should also note that the corresponding results for the antiferromagnetic Hartree–Fock solution match closely those obtained within the EDABI method, both for the *atomic* and for the *nanometallic* limits (particularly for the upper Hubbard band in the latter case). The electron–correlation effects, in contrast, appear clearly (near the Fermi momenta) for the intermediate range of  $R$ , where the Hartree–Fock charge gap is significantly larger than the exact one (cf. *preceding* Section). Another interesting feature of the renormalized dispersion relation is that the datapoints for different  $N$  ( $= 10$  and 12) compose a single (*universal*) dispersion curve  $\tilde{\epsilon}_{\mathbf{k}}$  provided that the proper boundary conditions, which minimize the ground-state energy for a particular  $N$ , are applied. The results for  $\tilde{\epsilon}_{\mathbf{k}}$  and those for the distribution func-

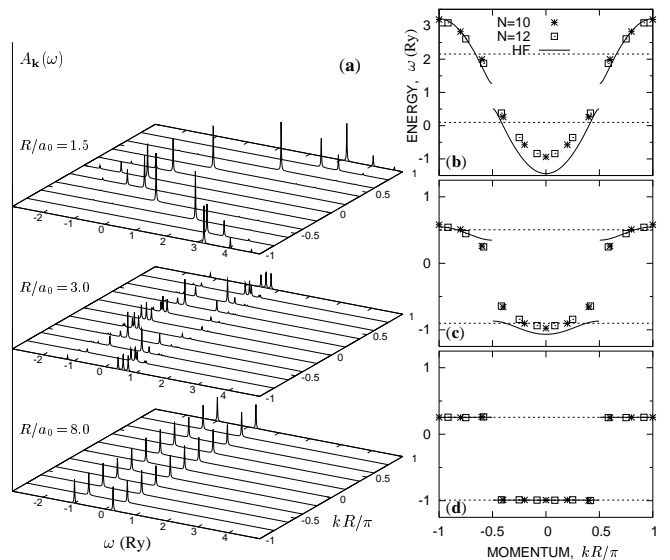


**Fig. 9.** Spectral functions  $A_{\mathbf{k}}(\omega)$  for the nanochain of  $N = 10$  atoms (a) and the corresponding renormalized dispersion relations for the lattice parameter  $R = 1.5a_0$  (b),  $R = 3a_0$  (c), and  $R = 8a_0$  (d). The quasiparticle energies for *antiferromagnetic* Hartree–Fock solution (solid lines) are also shown for the comparison.

tion  $n_{\mathbf{k}\sigma}$  (cf. Fig. 2a) characterize in a *fundamental manner* the salient features of electronic states for the *quantum nanoliquid*. They are supplemented with the results for the transport properties, which are considered next.

### 4.3 Drude weight and optical conductivity

The real part of the optical conductivity at zero temperature is determined by the corresponding real part of the linear response to the applied electric field [19] and can be written as  $\sigma(\omega) = D\delta(\omega) + \sigma_{\text{reg}}(\omega)$ , where the regular part is

$$\sigma_{\text{reg}}(\omega) = \frac{\pi}{N} \sum_{n \neq 0} \frac{|\langle \Psi_n | j_p | \Psi_0 \rangle|^2}{E_n - E_0} \delta(\omega - (E_n - E_0)), \quad (9)$$

whereas the Drude weight (the *charge stiffness*)  $D$  is defined by

$$D = -\frac{\pi}{N} \langle \Psi_0 | T | \Psi_0 \rangle - \frac{2\pi}{N} \sum_{n \neq 0} \frac{|\langle \Psi_n | j_p | \Psi_0 \rangle|^2}{E_n - E_0}, \quad (10)$$

with the kinetic–energy term  $T$  as the second term in Eq. (1) and the diamagnetic current operator defined as usual:  $j_p = it \sum_{j\sigma} (a_{j\sigma}^\dagger a_{j+1\sigma} - \text{HC})$ . Here the states  $|\Psi_n\rangle$  in Eqs. (9) and (10) are the eigenstates of Hamiltonian (1) corresponding to the eigenenergies  $E_n$ , again with the boundary conditions that minimize the ground–state energy for a given system size  $N$ . Matrix elements  $\langle \Psi_n | j_p | \Psi_0 \rangle$  are calculated within the Lanczos method [20]. For plotting purposes, we also use again the analytic representation of Dirac delta function  $\delta(x) \rightarrow (1/\pi)\epsilon/(x^2 + \epsilon^2)$ , with  $\epsilon = 0.01$  Ry.

For finite system of  $N$  atoms  $D$  is always nonzero due to a nonzero tunneling probability through a potential barrier of finite width. Because of that, the finite–size scaling with  $1/N \rightarrow 0$  has to be performed on  $D$ . Here we use, after Góra *et al.* [21], the following parabolic extrapolation

$$\ln |D_N^*| = a + b(1/N) + c(1/N)^2, \quad (11)$$

where  $D_N^*$  denotes the *normalized Drude weight*  $D^* = -(N/\pi)D/\langle \Psi_0 | T | \Psi_0 \rangle$  for the system of  $N$  sites, that provides the value in the range  $0 \leq D^* \leq 1$ , and thus can be regarded as an alternative order parameter for the transition to the localized (atomic) state.

The results for 1D system of  $N = 6 \div 14$  atoms in the *half-filled* chain case are shown in Fig. 10a. The values of  $D_N^*$  used for the scaling (11) are listed in Table 3, together with the resulting  $D_\infty^*$  and its relative error (we stop at the lattice parameter  $R$  for which  $D_\infty^* = 0$  within the range of errorbars). We also provide, for comparative purposes, the data for the system with the *on-site* Coulomb interaction only (i.e. for the Hubbard model) in Table 4. In both cases with the long–range (cf. Table 3) and the *on-site* only (cf. Table 4) interactions, the extrapolated Drude weight  $D_\infty^*$  becomes significantly greater than zero (of  $2\sigma$  value) only for small lattice parameter,  $R \leq 2.6a_0$  and

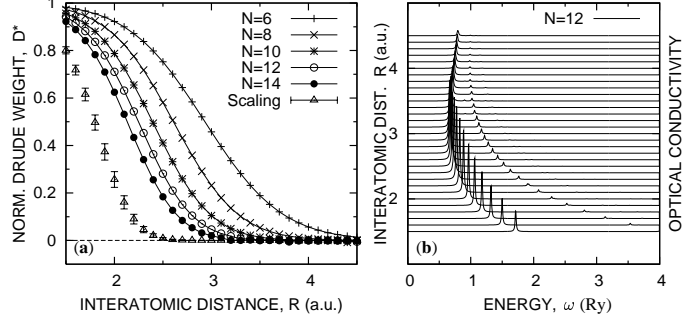


**Fig. 10.** Optical conductivity for nanochains in the *half-filled* case: (a) normalized Drude weight vs. lattice parameter  $R$  (specified in  $a_0$ ) and its values obtained through finite size scaling with  $1/N \rightarrow 0$ ; (b) regular part of the conductivity,  $\sigma_{\text{reg}}(\omega)$  for  $N = 12$  atoms.

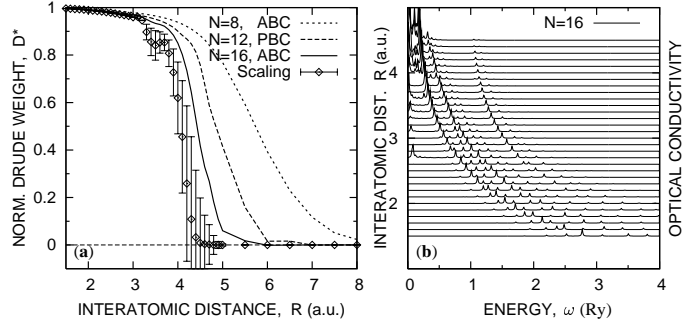


**Fig. 11.** Optical conductivity for the *quarter-filled* chain: (a) normalized Drude weight vs. lattice parameter  $R$  and its values extrapolated with  $1/N \rightarrow 0$  (the Aitken method has been used to estimate the errors); (b) regular part of the conductivity,  $\sigma_{\text{reg}}(\omega)$  for  $N = 16$  atoms.

$R \leq 2.1a_0$ , respectively. The limiting values match nicely those for which the Luttinger–liquid exponent crosses the critical value  $\theta = 1$ , corresponding to the localization–delocalization boundary. The above results suggest again the localization onset in these 1D systems at half–filling. However, the optical conductivity  $\sigma_{\text{reg}}(\omega)$ , drawn in Fig. 10b, shows the isolated Hubbard peak at  $\omega \approx U$  and *no intraband transitions* present in delocalized state. Because of this fact, and also because of the nonzero value of the charge–gap for any  $R$  (cf. *above*), one should regard both the half–filled systems studied here as the Mott insulators in the large  $N$  limit. Nevertheless, the finite– $N$  results show, that the conductivity of the nanoscopic chain diminishes by two orders of magnitude when the corresponding increase of the lattice parameter  $R$  is in the range of 40  $\div$  50%. So, one can consider such system as undergoing a transformation either from a *nanoliquid* to the *localized spin system* at the half–filling or from an intrinsically *partially localized* state, since the intraband transitions are absent even in the small– $R$  range. It would be very interesting to confirm experimentally these results.

The situation becomes again completely different at the *quarter–filling* (QF). Namely, the normalized Drude weight of the QF systems of  $N = 8 \div 16$  atoms, depicted

**Table 3.** Normalized Drude weight  $D_N^*$ , the extrapolated value  $D_\infty^*$ , and its relative error for 1D half-filled system with long-range Coulomb interaction.

$R/a_0$	$D_{14}^*$	$D_{12}^*$	$D_{10}^*$	$D_8^*$	$D_6^*$	$D_\infty^*$	$\sigma(D_\infty^*)/D_\infty^*$
1.5	0.9225	0.9420	0.9563	0.9727	0.9822	0.8008	0.019
2.0	0.6245	0.7105	0.7875	0.8660	0.9222	0.2567	0.129
2.5	0.1839	0.2812	0.4109	0.5813	0.7526	0.0087	0.420
2.6	0.1269	0.2096	0.3315	0.5065	0.7009	0.0033	0.489
2.7	0.0840	0.1508	0.2595	0.4312	0.6441	0.0012	0.566
3.0	0.0196	0.0461	0.1047	0.2314	0.4575	0.0000	—

**Table 4.** Normalized Drude weight  $D_N^*$ , the extrapolated value  $D_\infty^*$ , and its relative error for 1D half-filled system described by the Hubbard model.

$R/a_0$	$D_{14}^*$	$D_{12}^*$	$D_{10}^*$	$D_8^*$	$D_6^*$	$D_\infty^*$	$\sigma(D_\infty^*)/D_\infty^*$
1.5	0.6173	0.6742	0.7342	0.7973	0.8640	0.3294	0.070
2.0	0.1529	0.2259	0.3276	0.4631	0.6331	0.0092	0.364
2.1	0.0991	0.1598	0.2527	0.3884	0.5731	0.0032	0.449
2.2	0.0619	0.1094	0.1896	0.3190	0.5123	0.0010	0.540
2.5	0.0124	0.0294	0.0687	0.1561	0.3372	0.0000	—

in Fig. 11a, shows a *highly-conducting* behavior ( $D^* \approx 1$ ) for  $R \lesssim 3.5a_0$  and gradually transforms to zero in the range  $R/a_0 = 4 \div 5$ . Also, the regular part of conductivity  $\sigma_{\text{reg}}(\omega)$  (cf. Fig. 11b) comprises intraband transitions in the quasi-metallic range, particularly near the onset of the charge-density wave state (for  $N = 16$ ). Such a behavior provides the model case for the transformation from a nanometal in the small- $R$  range to the charge-ordered system (cf. Fig. 4) for larger  $R$ .

## 5 A brief overview: New features

We have provided a fairly complete description of electronic states in a finite 1D chain within the framework of EDABI method, which combines the *exact diagonalization* of many-fermion Hamiltonian in the Fock space with a subsequent *ab initio* readjustment of the single-particle (Wannier) functions. Both the ground-state and dynamical properties have been obtained as a function of the variable lattice parameter (interatomic spacing)  $R$ . Our approach thus *extends* the current theoretical treatments of band and strongly correlated systems within the parametrized (second-quantized) models by determining those parameters and, in turn, analyzing the correlated state explicitly as a function of  $R$ . The single-particle wavefunction is allowed to readjust in the correlated state within the EDABI method thus unifies the second and the first quantization aspects of the many-particle states into a single scheme.

We start from analyzing the situation with one valence electron per atom (the *half-filled* case) and includes the *long-range* Coulomb interaction. The Luttinger–liquid type of the electron momentum distribution suggests a *crossover transition* from the quasi-metallic to the insulating (spin-ordered) state with the increasing  $R$  (the

same is true about the system without the long-range interaction [13], but the quasi-metallic behavior is manifested to much stronger degree when the long-range part of the Coulomb interactions is included). The finite-size scaling with  $1/N \rightarrow 0$ , performed on the charge-energy gap shows the insulating nature of the ground state for the large  $N$  limit, in agreement with the renormalization-group results for the *infinite* system with two Fermi points [14]. Such an apparently dyadic nature (localized vs. itinerant) of the nanoscopic systems is confirmed by their transport properties. On one hand, the Drude weight is nonzero in the small  $R$  limit and the localization threshold agrees with those obtained from the Luttinger–liquid exponent, but the regular part of the optical conductivity exhibits the insulating behavior. This is the reason we coined the term: *partially localized quantum nanoliquid*. The most fundamental features of the electrons as a *quantum nanoliquid* is provided in Figs. 2a and 9b–d, where *Fermi-like* distribution, as well as the *renormalized band structure* appear for small interatomic spacing. These features evolve with  $R \rightarrow R_c$  into atomic-like through the regime with split Hubbard-like subbands.

An illustrative example of the nanoscopic system with a clear transformation from *nanometal* to *nanoinsulator* with the charge-density wave order is provided with the *quarter-filled* nanochain (when including again the long-range Coulomb interaction). For that system, the Drude weight is reduced gradually from its maximal value to zero and other properties evolve analogously with the increasing lattice parameter  $R$ . The intermediate range of  $R$ , where the crossover takes place, also shrinks rapidly with the increasing  $N$ , suggesting the existence of a sharp zero-temperature transition in the large  $N$  limit.

The above analysis, for both the half- and the quarter-filled cases is very sensitive to the choice of the boundary conditions. This problem is widely studied in the existing literature and its relation to the spontaneous magnetic

flux appearing in the mesoscopic rings of  $N = 4n$  atoms [22] has been established before [23].

The EDABI method implement here can be applied to discuss also the coupling of electrons the lattice and the dimerization (for a discussion see the third paper in Ref. [5]). Also, one should incorporate the properties of chain with odd number of electrons (the boundary conditions will involve then the complex number domain). Furthermore, the dynamics with single holes and impurities in the nanochain would make the system more realistic as a quantum wire. Finally, the application of the present scheme to the higher ( $ns$ -like) valence orbital systems would make possible a direct comparison with the experimental results quantum nanowires made of noble and alkaline elements. We should be able to see a progress along these lines soon.

### Acknowledgement

We thank our colleagues: Dr. Maciej Maśka and Prof. Krzysztof Rościszewski, for discussions about the Lanczos algorithm and the role of boundary conditions for finite systems. We are also grateful to the Institute of Physics of the Jagiellonian University for the support for computing facilities used in part of the numerical analysis. The support from the Committee for Scientific Research (KBN) of Poland (Grant No. 2P03B 050 23), and from the Foundation for Polish Science (FNP), is acknowledged. With this paper we would like to mark the European Union enlargement on May 1, 2004.

### References

1. P.C. Hohenberg, W. Kohn, L.I. Sham, in *Adv. Quantum Chemistry*, edited by S.B. Trickey, vol. 21 (Academic, San Diego, 1990), p. 7; W. Temmerman *et al.*, in *Electronic Density Functional Theory: Recent Progress and New Directions*, edited by J.F. Dobson *et al.* (Plenum, New York, 1998), p. 327
2. V.I. Anisimov, *et al.*, Phys. Rev. B **44**, 943 (1991); P. Wei and Z.Q. Qi, *ibid.* **49**, 10864 (1994)
3. A. Svane and O. Gunnarson, Europhys. Lett. **7**, 171 (1988); Phys. Rev. Lett. **65**, 1148 (1990)
4. S. Ezhov, *et al.*, Phys. Rev. Lett. **83**, 4136 (1999); K. Held *et al.*, *ibid.* **86**, 5345 (2001)
5. J. Spałek, *et al.* Phys. Rev. B **61**, 15676 (2001), and unpublished; A. Rycerz and J. Spałek, *ibid.* **63**, 073101 (2001); *ibid.* **65**, 035110 (2002); J. Spałek and A. Rycerz, *ibid.* **64**, R161105 (2001)
6. J. Spałek, *et al.*, Acta Phys. Polon. B **31**, 2879 (2000); *ibid.* **32**, 3189 (2001)
7. A. Rycerz, *et al.*, in *Lectures on the Physics of Highly Correlated Electron Systems VI*, edited by F. Mancini, AIP Conf. Proc. vol. 629 (New York, 2002) p. 213; *ibid.* vol. 678 (New York, 2003) p. 313
8. J. Spałek, *et al.*, in *Concepts in Electron Correlation*, Proc. NATO Adv. Res. Workshop, edited by A.C. Hewson and V. Zlatić (Kluwer, Dordrecht, 2003) p. 257
9. R. Resta, J. Phys. Condensed Matter **14**, R625 (2002); Phys. Rev. Lett. **80**, 1800 (1998); see also Resta and Sorella, Ref. [18]
10. A. Rycerz, *et al.*, Acta Phys. Polon. B **34**, 651 (2003); *ibid.* **655** (2003)
11. J. Solyom, Adv. Phys. **28**, 201 (1979); J. Voit, Rep. Prog. Phys. **57** 977 (1995)
12. S. Sorella, *et al.*, Europhys. Lett. **12**, 721 (1990)
13. A. Rycerz, Ph.D. Thesis, Jagiellonian University, Kraków, 2003
14. M. Fabrizio, Phys. Rev. B **54**, 10054 (1996); see also Voit, Ref. [11]
15. E.H. Lieb and F.Y. Wu Phys. Rev. Lett. **20**, 1445 (1968)
16. E.L. Altshuler, *et al.*, Phys. Rev. Lett. **78**, 2803 (1997)
17. W. Kohn, Phys. Rev. **133**, A171 (1964)
18. R. Resta and S. Sorella, Phys. Rev. Lett. **82**, 370 (1999); P. Korbel, *et al.*, Eur. Phys. J. B **32**, 315 (2003)
19. B.S. Shastry and B. Sutherland Phys. Rev. Lett. **65**, 243 (1990); J.A. Millis and S.N. Coppersmith, Phys. Rev. B **42**, 10807 (1990)
20. E. Dagotto, Rev. Mod. Phys. **66**, 763 (1994); P. Prelovšek and X. Zotos, in *Lectures on the Physics of Highly Correlated Electron Systems VI*, edited by F. Mancini, AIP Conf. Proc. vol 629 (New York, 2002) p. 161
21. D. Góra, K. Rościszewski, A.M. Oleś, J. Phys. Condensed Matter **10**, 4755 (1998)
22. M. Büttiker, *et al.*, Phys. Lett. **96A**, 365 (1983); R. Landauer and M. Büttiker, Phys. Rev. Lett. **54** 2049 (1985); D. Mailly, *et al.*, *ibid.* **70**, 2020 (1993)
23. M. Abraham, R. Berkovitz, Phys. Rev. Lett. **70**, 1509 (1993); G. Bouzerar, Phys. Rev. B **49**, 8258 (1994); J.-X. Zhu, Z.D. Wang, *ibid.* **52**, 14505 (1995)